RESEARCH ARTICLE

Correlation between TGF-β1 expression and proteomic profiling induced by severe acute respiratory syndrome coronavirus papain-like protease

Shih-Wen Li[1,2], Tsuey-Ching Yang[3], Lei Wan[4], Ying-Ju Lin[4], Fuu-Jen Tsai[4], Chien-Chen Lai[2,4] and Cheng-Wen Lin[1,5,6]*

[1] Department of Medical Laboratory Science and Biotechnology, China Medical University, Taichung, Taiwan
[2] Institute of Molecular Biology, National Chung Hsing University, Taichung, Taiwan
[3] Department of Biotechnology and Laboratory Science in Medicine, National Yang Ming University, Taipei, Taiwan
[4] Department of Medical Genetics and Medical Research, China Medical University Hospital, Taichung, Taiwan
[5] Clinical Virology Laboratory, Department of Laboratory Medicine, China Medical University Hospital, Taichung, Taiwan
[6] Department of Biotechnology, Asia University, Taichung, Taiwan

Received: June 5, 2012
Revised: July 20, 2012
Accepted: August 9, 2012

Severe acute respiratory syndrome (SARS) coronavirus (SARS-CoV) papain-like protease (PLpro), a deubiquitinating enzyme, demonstrates inactivation of interferon (IFN) regulatory factor 3 and NF-κB, reduction of IFN induction, and suppression of type I IFN signaling pathway. This study investigates cytokine expression and proteomic change induced by SARS-CoV PLpro in human promonocyte cells. PLpro significantly increased TGF-β1 mRNA expression (greater than fourfold) and protein production (greater than threefold). Proteomic analysis, Western blot, and quantitative real-time PCR assays indicated PLpro upregulating TGF-β1-associated genes: HSP27, protein disulfide isomerase A3 precursor, glial fibrillary acidic protein, vimentin, retinal dehydrogenase 2, and glutathione transferase omega-1. PLpro-activated ubiquitin proteasome pathway via upregulation of ubiquitin-conjugating enzyme E2–25k and proteasome subunit alpha type 5. Proteasome inhibitor MG-132 significantly reduced expression of TGF-β1 and vimentin. PLpro upregulated HSP27, linking with activation of p38 MAPK and ERK1/2 signaling. Treatment with SB203580 and U0126 reduced PLpro-induced expression of TGF-β1, vimentin, and type I collagen. Results point to SARS-CoV PLpro triggering TGF-β1 production via ubiquitin proteasome, p38 MAPK, and ERK1/2-mediated signaling.

Keywords:
Microbiology / Papain-like protease / SARS coronavirus / TGF-β1 / Ubiquitin proteasome / Vimentin

1 Introduction

Severe acute respiratory syndrome (SARS) associated coronavirus (SARS-CoV) is a causative agent of severe and atypical pneumonia [1, 2] that caused a global outbreak in 2003, resulting in over 8000 probable cases with a mortality of some 10%. Clinical pathology indicates bronchial epithelial denudation, multinucleated syncytial cells, loss of cilia, squamous metaplasia, inflammation infiltration of monocytes, macrophages, and neutrophils into lung tissue [2, 3]. Clinical laboratory examination reveals SARS-CoV triggering lymphopenia, thrombocytopenia, and leucopenia [4, 5] while rapidly elevating serum of inflammatory cytokines, e.g. IFN-γ, IL-18, TGF-β1, TNF-α, IL-6, IP-10, MCP-1, MIG, and IL-8 [6, 7]. SARS-CoV-induced proinflammatory

Correspondence: Prof. Dr. Cheng-Wen Lin, Department of Medical Laboratory Science and Biotechnology, China Medical University, No. 91, Hsueh-Shih Road, Taichung 404, Taiwan
E-mail: cwlin@mail.cmu.edu.tw
Fax: 886-4-22057414

Abbreviations: CoV, Coronavirus; **EMT**, epithelial–mesenchymal transdifferentiation; **ERK**, extracellular signal-regulated kinase; **IFN**, interferon; **MAPK**, mitogen-activated protein kinase; **NS**, nonstructural; **OAS**, oligoadenylate synthetase; **RANTES**, regulated and normal T cell expressed and secreted; **SARS**, severe acute respiratory syndrome; **TNFR**, tumor necrosis factor receptor; **TRAF**, TNFR-associated factor

*Additional corresponding author: Professor Chien-Chen Lai, E-mail: lailai@dragon.nchu.edu.tw

Colour Online: See the article online to view Figures 1, 4, and 8 in colour.

cytokine storms are linked with recruitment of neutrophils, monocytes, and immune responder cells such as natural killer, T, and B cells into the lungs, resulting in acute lung injury, acute respiratory distress syndrome, even lung fibrosis in the late phase [7].

SARS-CoV genome is an approximately 30 kbp positive-stranded RNA with a 5′ cap and 3′ poly(A) tract, containing 14 ORFs [8, 9]. Polyprotein replicases 1a and 1ab (∼450 and ∼750 kDa, respectively) encoded by 5′ proximal, producing nonstructural (NS) proteins primarily involved in RNA replication. Specifically, papain-like protease (PLpro) and 3C-like protease, two embedded proteases, mediate the processing of 1a and 1ab precursors into 16 NS proteins (termed NS 1 through NS16). PLpro recognizes a consensus motif LXGG as consensus cleavage sequence of cellular deubiquitinating enzymes, and cleaves polyprotein replicase 1a at NS1/2, NS2/3, and NS3/4 boundaries [10, 11]. Modeling with crystal structures of herpes virus associated ubiquitin-specific protease and in vitro cleavage assays reveal SARS-CoV PLpro as a deubiquitinating enzyme [12, 13]. These in vitro de-ubiquination assays illustrate cleavage of interferon (IFN)-induced 15-kDa protein (ISG15)-conjugated proteins by PLpro [12, 13]. Deubiquitinating/de-ISGylating activity of PLpro is believed to link with a mechanism that SARS-CoV infection induces on type I IFNs in cell culture [14]. PLpro is further identified by blocking type I IFN synthesis through inhibiting phosphorylation of IFN regulatory factor 3 [15]. PLpro antagonizes type I IFN signaling pathway by polyubiquitination and degradation of extracellular signal-regulated kinase 1 (ERK1), resulting in the inhibition of STAT1 phosphorylation and decrease of IFN-stimulated gene expression such as PKR, 2′-5′-oligoadenylate synthetase (OAS), IL-6, and IL-8 [16]. A deubiquitinating enzyme cylindromatosis that inhibits NF-κB signaling via deubiquitination and inactivation of tumor necrosis factor receptor (TNFR)-associated factor 2 (TRAF2) and TRAF6 [17] has been reported to promote inflammatory responses via mitogen-activated protein kinase (MAPK)-mediated but NF-κB independent pathways [18]. Deubiquitinating protease A20 inhibits TLR4-mediated NF-κB activation, directly removing K63-linked polyubiquitin chains of TRAF6 while reducing production of antiviral and proinflammatory cytokines by inactivation of RIG-I dependent antiviral signaling [19]. Yet the role of deubiquitinating enzyme PLpro in anti-inflammation and proinflammatory response remains unclear. This study assesses possible effect of SARS-CoV PLpro on cytokine induction: TGF-β1, TNF-α, IFN-β, IL-1α, regulated and normal T cell expressed and secreted protein (RANTES). Comparative proteomic analysis of PLpro expressing versus vector control cells yielded data on the relation between TGF-β1 production and protein expression change induced by PLpro, affording insights into molecular mechanism(s) of SARS pathogenesis.

2 Materials and methods

2.1 Cell culture and transfection

SARS-CoV PLpro gene amplified by RT-PCR was cloned into pcDNA3.1/HisC vector (Invitrogen) as described in our previous report [16]. This resulting construct pSARS-PLpro (4.5 μg) or pcDNA3.1 empty vector was transfected into HL-CZ cells, a human promonocyte cell line, using GenePorter reagent. Stable transfected cells were generated through long-period incubation with RPMI-1640 medium containing 10% FBS and 800 μg/mL of G418. To analyze expression, cells transfected with pSARS-PLpro or empty vector were washed once in PBS, then fixed in 3.7% formaldehyde in PBS for 1 h. Cells subsequently underwent 1-h incubation with anti-PLpro sera from mice immunized with *E. coli*-synthesized PLpro, followed by another 1-h incubation with FITC-conjugated antimouse IgG antibody (Abcam). Finally, cells were stained with 4′,6-diamidino-2-phenylindole (DAPI, Sigma) for 10 min. After three PBS washes, imaging was analyzed by immunofluorescent microscopy (Olympus, BX50).

2.2 Western blot assay

To resolve protein expression, lysates of PLpro-expressing and empty vector control cells were mixed in the ratio of 1:1 with 2× SDS-PAGE sample buffer, then boiled for 10 min. Proteins in cell lysates were detected by SDS-PAGE and transferred to nitrocellulose. After blocking with 5% skim milk, resulting blots were reacted with properly diluted antibodies, e.g. rabbit antivimentin (GeneTex), anti-PLpro mouse sera, rabbit anti-ERK1/2 (Cell signaling), rabbit antiphospho-ERK1/2 (Thr202/Tyr204) (Cell signaling), anti-HSP27 mAb (Chemicon), and anti-β-actin mAb (Abcam). Immune complexes were detected with HRP-conjugated goat antimouse or antirabbit IgG antibodies, followed by enhanced chemiluminescence detection (Amersham Pharmacia Biotech).

2.3 Quantitative RT-PCR

Total RNA was extracted from stable transfected cells with pSARS-PLpro or empty vector incubated for 4 h in the presence or absence of 3000 U/mL IFN-α, 20 μM MG-132 (a proteasome inhibitor) or 15 μM U0126 (an ERK1/2 inhibitor), using PureLink Micro-to-Midi Total RNA Purification System kit (Invitrogen). Two-step real-time RT-PCR using SYBR Green I quantified expression in response to SARS PLpro; cDNA was synthesized from 1 μg total RNA, using oligonucleotide d(T) primer and SuperScript III reverse transcriptase kit (Invitrogen), as previously described [16]. Real-time PCR mixture contained 5 μL of a cDNA mixture, 1 μL of primer pair (200 nM, Supporting Information Table S1), and 12.5 μL Smart Quant Green Master Mix with Dutp and ROX (Protech). PCR was performed with amplification protocol

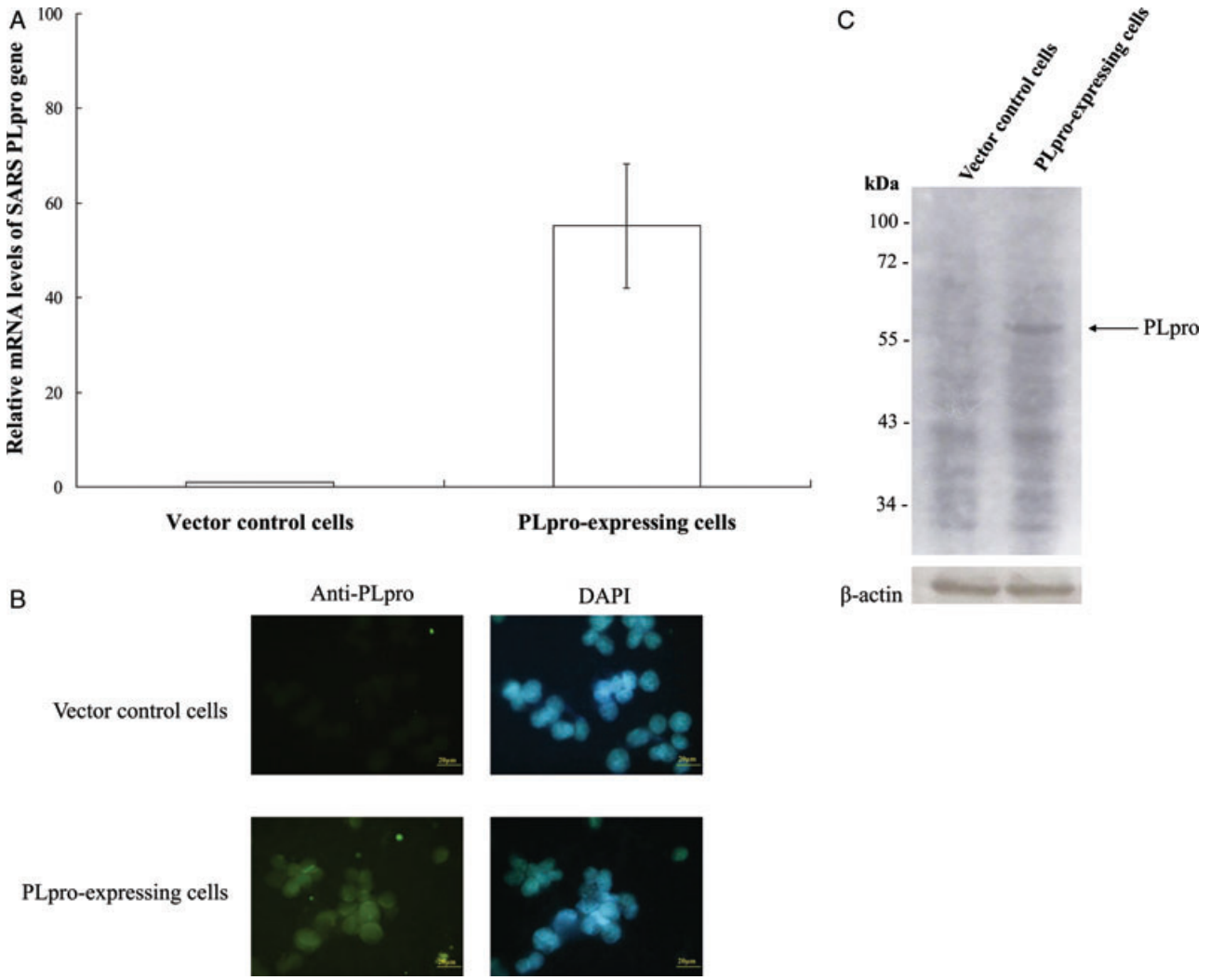

Figure 1. Expression of SARS-CoV PLpro in human promonocyte HL-CZ cells. (A) Relative mRNA level of SARS-CoV PLpro in transfected cells was measured by quantitative real-time PCR and normalized by GAPDH mRNA. (B, C) Recombinant PLpro protein in transfected cells was detected by immunofluorescent staining, its molecular weight analyzed by Western blot. Lysates from cells transfected with pcDNA3.1 (lane 1) or pSARS-PLpro (lane 2) were analyzed by 10% SDS-PAGE prior to blotting; resulting blot was probed with mouse polyclonal sera against *E. coli*-synthesized PLpro (top) and anti-β actin monoclonal antibody as internal control.

consisting of 1 cycle at 50°C for 2 min, 1 cycle at 95°C for 10 min, 40 cycles at 95°C for 15 s, and 60°C for 1 min. Amplification and detection of specific products were conducted in ABI Prism 7900 sequence detection system (PE Applied Biosystems). Relative changes in mRNA level of indicated genes were normalized relative to GAPDH mRNA.

2.4 ELISA analysis of TGF-β1 in cultured medium and cell lysates

Those 2×10^6 vector control or PLpro-expressing cells were treated with/without 20 μM MG-132, 15 μM U0126, or 5 μM SB203580 (a p38 MAPK inhibitor) in 5 mL of serum-free medium for 1 day, 400 μL of each cultured medium and cell lysates mixed with 40 μL of coating buffer; 100 μL of each mixture was immediately coated into a 96-well plate at 4°C for 1 day. After tris-buffered saline and Tween-20 (TBST) washing, the 96-well plate was blocked in 1% BSA in TBST for 1 h at room temperature, incubated with 1:2000 dilutions of rabbit anti-TGF-β1 antibodies (Cell Signaling) for 2 h, then reacted with HRP-conjugated goat antirabbit IgG (Sigma) for another 1 h. Relative TGF-β1 protein level was ascertained by chromogen solution of hydrogen peroxide and 2,2′-azinodi-3-ethylbenzthiazoline-6-sulfonate, colored product at OD_{405nm} detected by ELISA reader (BioTek, Elx808).

2.5 2DE and protein spot analysis

For 2DE as described in our prior reports [16], total proteins from vector control and PLpro-expressing cells were

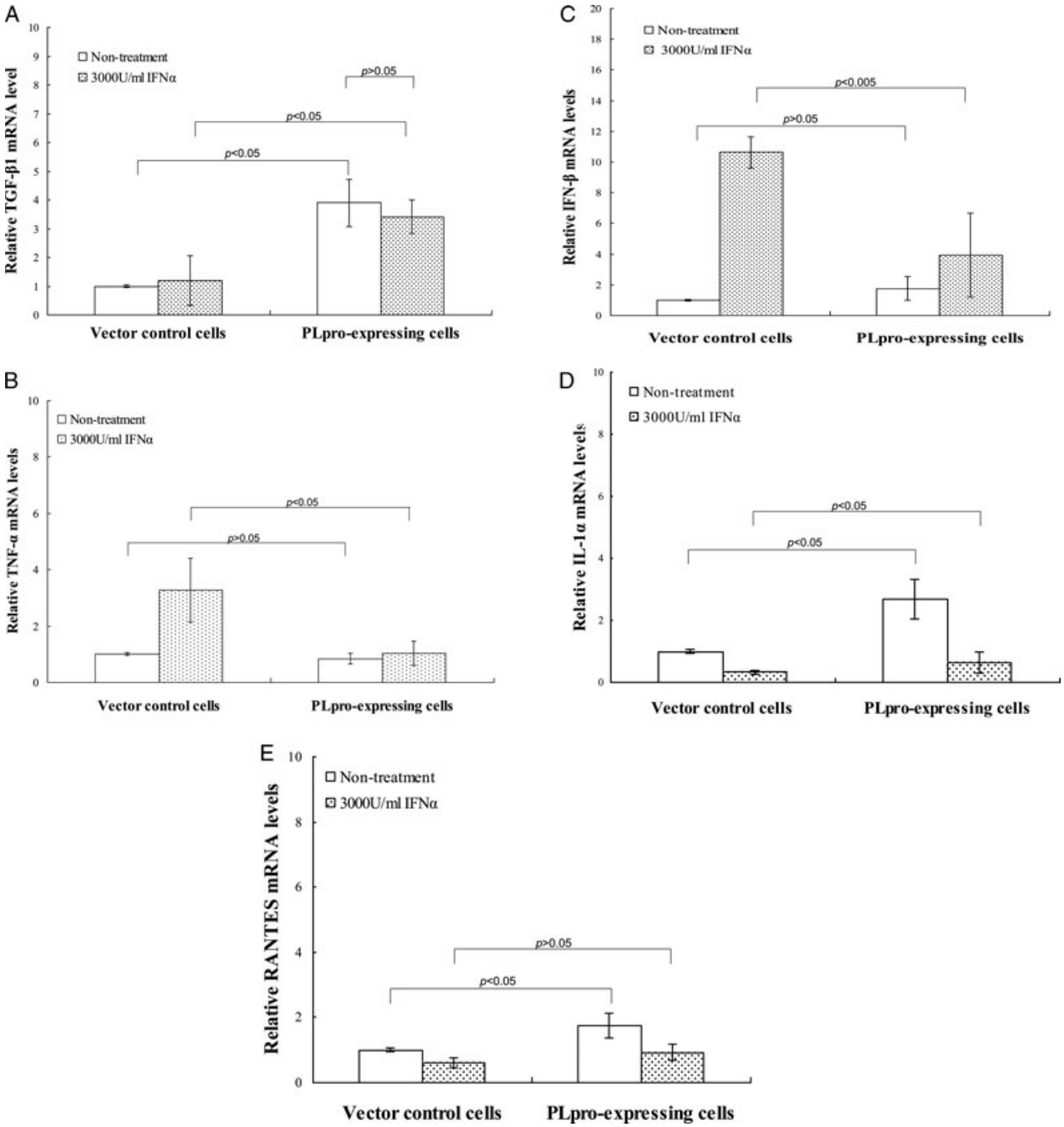

Figure 2. Cytokine mRNA expression in vector control and PLpro-expressing cells treated with and without IFN-α. Vector control and PLpro-expressing cells were treated with or without IFN-α in 4 h, mRNA expression of cytokine gene in cells untreated or treated measured by quantitative PCR. Relative mRNA levels of (A) TGF-β1, (B) TNF-α, (C) IFN-β, (D) IL-1α, and (E) RANTES were normalized by GAPDH mRNA, presented as relative ratio.

harvested, 100 μg of protein sample diluted with 350 μL of rehydration buffer, and applied to nonlinear Immobiline DryStrips (17 cm, pH 3–10; GE Healthcare), then applied for first-dimensional isoelectric focusing, using Multiphor II system (GE Healthcare) and 2DE using 12% polyacrylamide gels (20 cm × 20 cm × 1.0 mm). Gels were fixed in 40% ethanol, 10% glacial acetic acid for 30 min, stained with silver nitrate solution for 20 min, then scanned by GS-800 imaging densitometer with PDQuest software version 7.1.1 (Bio-Rad). Three independent lysates under each condition served for the correction of spot intensity graphs and statistical analysis.

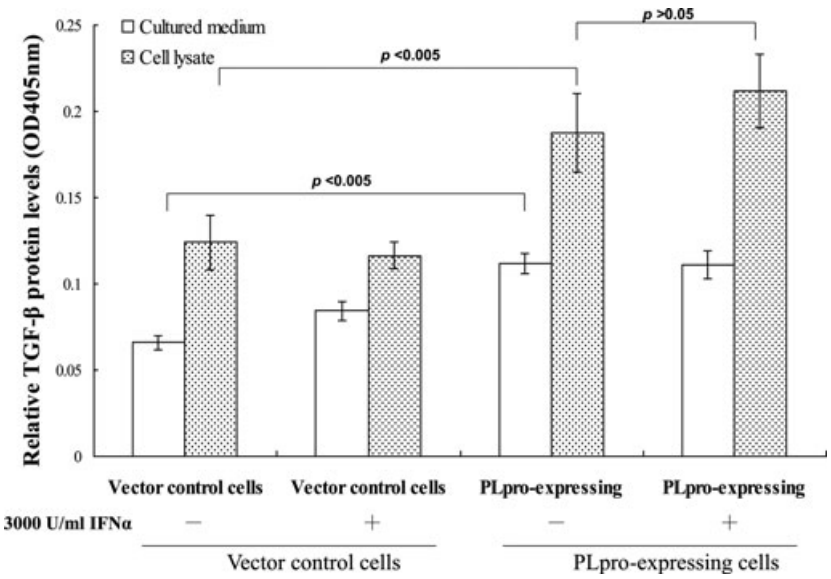

Figure 3. Protein levels of TGF-β1 in cultured media and lysates of PLpro-expressing and vector control cells with or without IFN-α. Vector control or PLpro-expressing cells treated with or without 3000 U/mL IFN-α were incubated in serum-free medium for 1 day. Cultured media or cell lysate were coated into wells of a 96-well plate at 4°C overnight, then reacted with rabbit anti-TGF-β1 antibodies and HRP-conjugated goat antirabbit IgG. The colored product was detected at $OD_{405\,nm}$.

2.6 In-gel digestion, nanoelectrospray MS, and database search

In-gel digestion recovered peptides from gel spots for nanoelectrospray MS, as described in our prior reports [16, 20]. Excised spots were soaked in 100% ACN for 5 min, dried in lyophilizer for 30 min, and rehydrated in 50 Mm ammonium bicarbonate buffer (pH 8.0) containing 10 μg/mL trypsin, followed by incubation at 30°C for 16 h. Digested peptides were extracted from supernatant of gel digestion solution (50% ACN in 5.0% trifluoroacetic acid) and dried in vacuum centrifuge. Peptides from digested protein spots were separated by RP C18 capillary column (flow rate 200 nL/min) and eluted with linear (10–50%) ACN gradient in 0.1% formic acid for 60 min. Eluted peptides from the capillary column were electrosprayed into mass spectrometer by PicoTip (FS360–20-10-D-20; New Objective, Cambridge, MA, USA), data acquisition from Q-TOF operated in data-dependent mode to measure MS and MS^2, using automatic Information Dependent Acquisition software (IDA; Applied Biosystem/MDS Sciex). The three most intense ions were sequentially isolated and fragmented in Q-TOF by collision-induced dissociation. Derived peak list generated by Mascot.dll v1.6b27 (Applied Biosystems) was searched as previously described [21] with a local version of the Mascot (2) program (v2.2.1; Matrix Science Ltd) and Mascot Daemon application (v2.2.0); parameters as follows: peptide and MS/MS tolerance, ±0.3 Da; trypsin missed cleavages, 1; variable modifications, carbamidomethylation and Met oxidation; and instrument type, ESI-Q-TOF. Protein identification was based on assignment of at least two peptides, protein function and subcellular location annotated by Swiss-Prot (http://us.Expasy.org/sprot/). Proteins were also categorized according to biological process and pathway via PANTHER (Protein Analysis Through Evolutionary Relationships) classification (http://www.pantherdb.org) described in prior studies [5, 22–24].

2.7 Statistical analysis

Each bar on the graph shows the mean of three independent experiments; error bars represent standard error of the mean. Chi-square and student's *t*-test analyzed all data, statistical significance between types of cells noted at $p < 0.05$.

3 Results

3.1 SARS-CoV PLpro-induced TGF-β1 production in human promonocytes

PLpro was expressed in promonocyte cells transfected with recombinant plasmid containing SARS-CoV PLpro gene. After two-week selection with G418, quantitative real-time PCR showed significant expression of PLpro mRNA in transfected versus control cells (Fig. 1A). Immunofluorescent staining with sera from hyper-immunized mice with recombinant PLpro protein indicated immunoreactive fluorescence in transfected as opposed to empty vector cells (Fig. 1B). Western blot analysis with sera of mice hyper-immunized with *E.coli*-synthesized PLpro identified a 60-kDa band recombinant PLpro protein in transfected cells but not controls (Fig. 1C), indicating SARS-CoV PLpro stably expressed in human promonocyte cells.

Because PLpro suppressed IFN-α signaling pathway via inactivation of ERK1 and STAT1 [16], effect of SARS-CoV PLpro expression on cytokine production (TGF-β1, TNF-α, IL-1α, IFN-β, and RANTES) was further characterized via SYBR Green real-time PCR (Fig. 2). Cytokine mRNA levels in PLpro-expressing and vector control cells were quantified and then normalized to housekeeping gene GAPDH expression. PLpro alone induced mRNA expression of TGF-β1 (greater than fourfold), IL-1α (approximately threefold), and RANTES

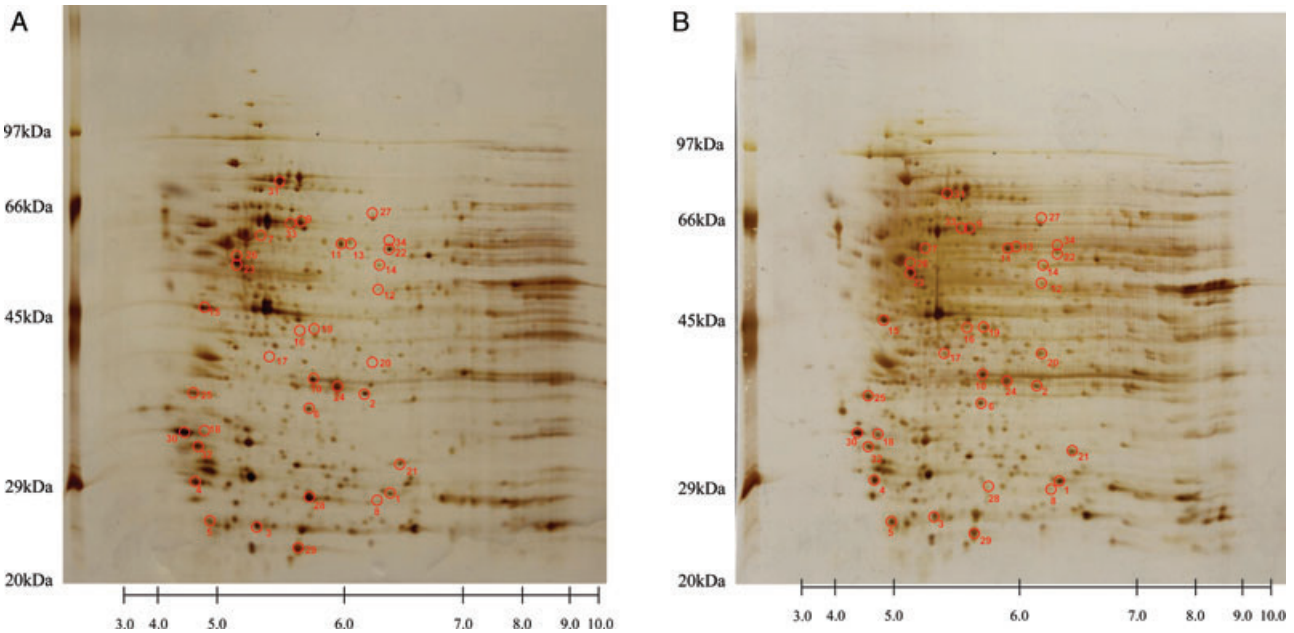

Figure 4. Silver stain of 2D gel of PLpro-expressing and vector control cells. Total protein of 100 μg from (A) vector control cells or (B) PLpro-expressing cells was applied to the nonlinear Immobiline DryStrip (17 cm, pH 3–10) and transferred to the top of 12% polyacrylamide gels (20 × 20 cm × 1.0 mm). Protein size markers are shown at the left of each gel (in kDa).

(approximately twofold) (Fig. 2A, D, and E), yet no significant rise in TNF-α and IFN-β compared to vector controls (Fig. 2B and C). IFN-α treatment stimulated higher transcriptional levels of TNF-α and IFN-β, but not TGF-β1, IL-1α, and RANTES in vector controls than in PLpro-expressing cells (Fig. 2). To confirm PLpro-induced TGF-β1 expression, cultured media and lysates were harvested from identical amounts of vector control and PLpro-expressing cells grown with FBS-free medium for 24 h, coated into 96-well plates for ELISA assay with rabbit anti-TGF-β1 Ab (Fig. 3). TGF-β1 in cultured media and cell lysates of PLpro-expressing cells were twice as high as in vector controls, indicating that PLpro plays a unique role in upregulating TGF-β1 production.

3.2 Proteomic analysis of expression profiles induced by SARS-CoV PLpro

To differentiate specific protein profiling induced by PLpro, protein expression between vector control and PLpro-expressing cells was analyzed by 2DE (Fig. 4): 34 protein spots (>1.5-fold change in spot intensity) identified by trypsin digestion and nanoscale capillary LC/ESI-Q-TOF MS. Identified proteins matched with Mascot score above 75; MW and *p*I of indicated proteins in 2DE gel (Fig. 4, Tables 1 and 2). Amino acid sequence coverage of identified proteins varied (4–71%). MS analysis of HSP27 (Spot ID 1) showed a Mascot score of 161, five matched peptides, and sequence coverage of 37%; vimentin (Spot ID 7) showed a Mascot score of 1420, sequence coverage of 71%, and 14 matched peptides. Peptide peaks from Q-TOF MS analysis from three representative spots of interest, vimentin (Spot ID 7), glial fibrillary acidic protein (Spot ID 17), and HSP27 (Spot ID 1) appear in Supporting Information Fig. S1A–C. Analyzing cell lysates by Western blot confirms protein profiling induced by PLpro (Fig. 5), i.e. significant rise of vimentin and HSP27 coupled with substantial decline of ERK1 in PLpro-expressing cells compared to vector controls, consistent with 2DE/Q-TOF MS/MS analysis in Fig. 4, Tables 1 and 2. Moreover, quantitative real-time PCR indicated mRNA expression of ubiquitin-conjugating enzyme E2–25 kDa (Spot ID 3) and protein disulfide isomerase A3 precursor (Spot ID 11) upregulated twofold in PLpro-expressing cells, but no change in controls (Supporting Information Fig. S2), supporting 2D/MS data (Fig. 4 and Table 1). Thus, 21 up- and 13 downregulated proteins were identified in PLpro-expressing cells.

3.3 Inhibition of ubiquitin proteasome activity reduces PLpro-induced expression of TGF-β1 and vimentin

To examine the effect of PLpro-induced activation of ubiquitin proteasome pathway via UBE2K upregulation of TGF-β1 and vimentin expression, cells were analyzed for protein and mRNA of TGF-β1 and vimentin with or without proteasome inhibitor MG-132 (Fig. 6). Quantitative real-time PCR assay indicated MG-132 causing more than a twofold decrease

Table 1. Upregulated proteins in PLpro-expressing cells compared to vector control cells

Spot ID	PANTHER gene ID	Protein identification	Mascot score	MW / p*I*	Numbers of peptides identified	Sequence coverage (%)	Fold change		Subcellular location
							Mean	SD	
1	3315	Heat-shock protein 27 (HSP27)	161	22.8/5.98	5	37	2.5	0.6	Cytoplasm, nucleus
2	23475	Nicotinate-nucleotide pyrophosphorylase [carboxylating] (QPRT)	238	30.8/5.81	4	43	1.54	0.13	Cytosol
3	3093	Ubiquitin-conjugating enzyme E2–25 kDa (UBE2K)	248	22.4/5.33	4	59	1.56	0.11	Cytoplasm
4	5686	Proteasome subunit alpha type 5 (PSA5)	157	26.4/4.74	4	30	1.68	0.15	Cytoplasm, nucleus
5	7178	Translationally controlled tumor protein (TCTP)	244	19.6/4.84	3	28	1.66	01656	Cytoplasm
6	5464	Inorganic pyrophosphatase (IPYR)	143	32.6/5.54	2	13	1.52	0.2	Cytoplasm
7	7431	Vimentin (VIM)	1420	53.6/5.06	14	71	1.63	0.1	Cytoplasm, cytoskeleton
8	9588	Peroxiredoxin-6 (PRDX6)	97	25/6.0	4	24	2.675	1.015	Cytoplasm, lysosome, cytoplasmic vesicle
9	22948	T-complex protein 1 subunit epsilon (CCT5)	702	59.6/5.45	8	32	1.838	0.045	cytoplasm, cytoskeleton, centrosome
10	6175	60S acidic ribosomal protein P0 (RPLP0)	517	34.3/5.71	5	41	1.69	0.165	Nucleus, cytoplasm
11	2923	Protein disulfide isomerase A3 precursor (PDIA3)	736	56.7/5.98	11	35	2.4	0.75	Endoplasmic reticulum lumen, melanosome
12	1832	Desmoplakin (DSP)	440	331.6/6.44	13	11	2.168	0.373	Cell junction, desmosome, cytoplasm, cytoskeleton
13	8854	Retinal dehydrogenase 2 (ALDH1A2)	630	56.7/5.79	10	29	2.561	0.181	Cytoplasm
14	3187	Heterogeneous nuclear ribonucleoprotein H (HNRNPH1)	233	49.2/5.89	6	21	9.469	1.627	Nucleus, nucleoplasm
15	3921	40S ribosomal protein SA (RPSA)	617	32.8/4.79	5	39	11.7	0.1	Cell membrane, cytoplasm, nucleus
16	3728	Junction plakoglobin (JUP)	174	81.6/5.95	7	9	1.77	0.35	Cell junction adherens junction, desmosome, cytoplasm, peripheral membrane protein
17	2670	Glial fibrillary acidic protein (GFAP), astrocyte	297	49.9/5.42	3	6	3.44	0.44	Cytoplasm, cytoskeleton
18	7170	Tropomyosin alpha-3 chain (TPM3)	264	32.8/4.68	3	27	3.2	0.252	Cytoplasm, cytoskeleton
19	213	Serum albumin precursor (ALB)	124	69.3/5.92	4	10	3.6	1.9	Secreted
20	117159	Dermcidin precursor (DCD)	70	11.2/6.08	2	22	2.51	0.65	Secreted
21	9446	Glutathione transferase omega-1 (GSTO1)	92	27.5/6.23	6	28	1.57	0.06	Cytoplasm

Table 2. Downregulated proteins in PLpro-expressing cells compared to vector control cells

Spot ID	PANTHER gene ID	Protein identification	Mascot score	MW / p*I*	Numbers of peptides identified	Sequence coverage (%)	Fold change		Subcellular location
							Mean	SD	
22	7453	Tryptophanyl-tRNA synthetase (WARS2)	606	53.1 / 5.83	10	33	0.545	0.235	Mitochondrion matrix
23	10130	Protein disulfide-isomerase A6 precursor (PDIA6)	227	48.1/4.95	9	25	0.44	0.14	Endoplasmic reticulum lumen, cell membrane, melanosome
24	3945	L-lactate dehydrogenase B chain (LDHB)	498	36.6/5.71	7	35	0.455	0.095	Cytoplasm
25	5111	Proliferating cell nuclear antigen (PCNA)	385	28.8/4.57	6	50	0.562	0.108	Nucleus
26	506	ATP synthase subunit beta, mitochondrial precursor (ATP5E)	685	56.5 / 5.26	9	34	0.333	0.006	Mitochondrion, mitochondrion inner membrane
27	5595	Mitogen-activated protein kinase 3 (ERK1)	109	43.1/6.28	2	14	0.195	0.077	Cytosol
28	4722	NADH dehydrogenase (NDUFC2)	182	30.2/6.99	2	10	0.257	0.043	Mitochondrion inner membrane
29	7001	Peroxiredoxin-2 (PRDX2)	290	21.9/5.66	3	22	0.53	0.03	Cytoplasm
30	1933	Elongation factor 1-beta (EEF1B2)	353	24.7/4.5	4	53	0.341	0.18	Cytosol
31	3312	Heat-shock cognate 71 kDa protein (HSC70)	775	70.9/5.37	11	33	0.457	0.133	Cytoplasm, melanosome
32	7531	14–3-3 protein epsilon (YWHAE)	681	29.1/4.63	6	67	0.251	0.014	Cytoplasm, melanosome
33	2324	Vascular endothelial growth factor receptor 3 (VEGFR3) precursor	146	145.5/5.89	3	4	0.507	0.264	Cell membrane, single-pass type I membrane protein, cytoplasm, nucleus
34	10376	Tubulin alpha-ubiquitous chain (Alpha-tubulin ubiquitous) (TUBA1B)	75	50.1/4.94	1	3	0.335	0.058	Cytoplasm, cytoskeleton

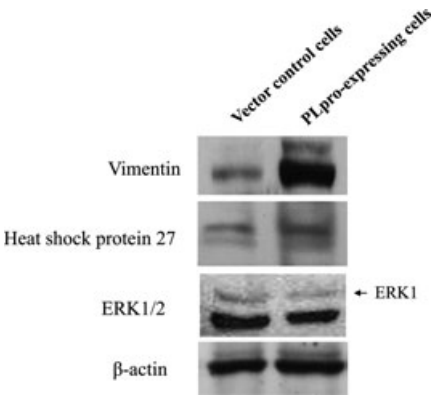

Figure 5. Western blot analysis of vimentin, HSP27, and ERK1/2 in vector control and PLpro-expressing cells. Lysates from vector control and PLpro-expressing cells were analyzed by 10% SDS-PAGE prior to blot. Resulting blot was probed with antivimentin, anti-ERK1/2, anti-HSP27, and anti-β actin antibodies, followed by enhanced chemiluminescence detection.

of TGF-β1 and vimentin mRNA in PLpro-expressing versus control cells (Fig. 6A). ELISA assays indicated MG-132 reducing TGF-β1 protein in lysates of PLpro-expressing cells by twofold and no effect on controls (Fig. 6B), proving ubiquitin–proteasomal system involvement in PLpro-induced expression of TGF-β1 and vimentin.

3.4 SB203580 and U0126 reduce PLpro-induced expression of TGF-β1 and vimentin

To ascertain whether p38 MAPK and ERK1/2 signaling pathways linked with PLpro-induced expression of TGF-β1 and vimentin, treatment with(out) p38 MAPK inhibitor SB203580 and ERK1/2 inhibitor U0126 was further analyzed by ELISA and quantitative real-time PCR assays (Fig. 7). ELISA assay showed less PLpro-induced TGF-β1 production by SB203580 (1.5-fold) and U0126 (3.3-fold) (Fig. 7A and B). Quantitative real-time PCR assay indicated U0126 raising PLpro-induced mRNA expression of TGF-β1 (sixfold), vimentin (3.3-fold), and type I collagen (8.4-fold) (Fig. 7C). Results indicated the activation of p38 MAPK- and ERK1/2-mediated signaling linking with induction of TGF-β1 and upregulation of vimentin by PLpro.

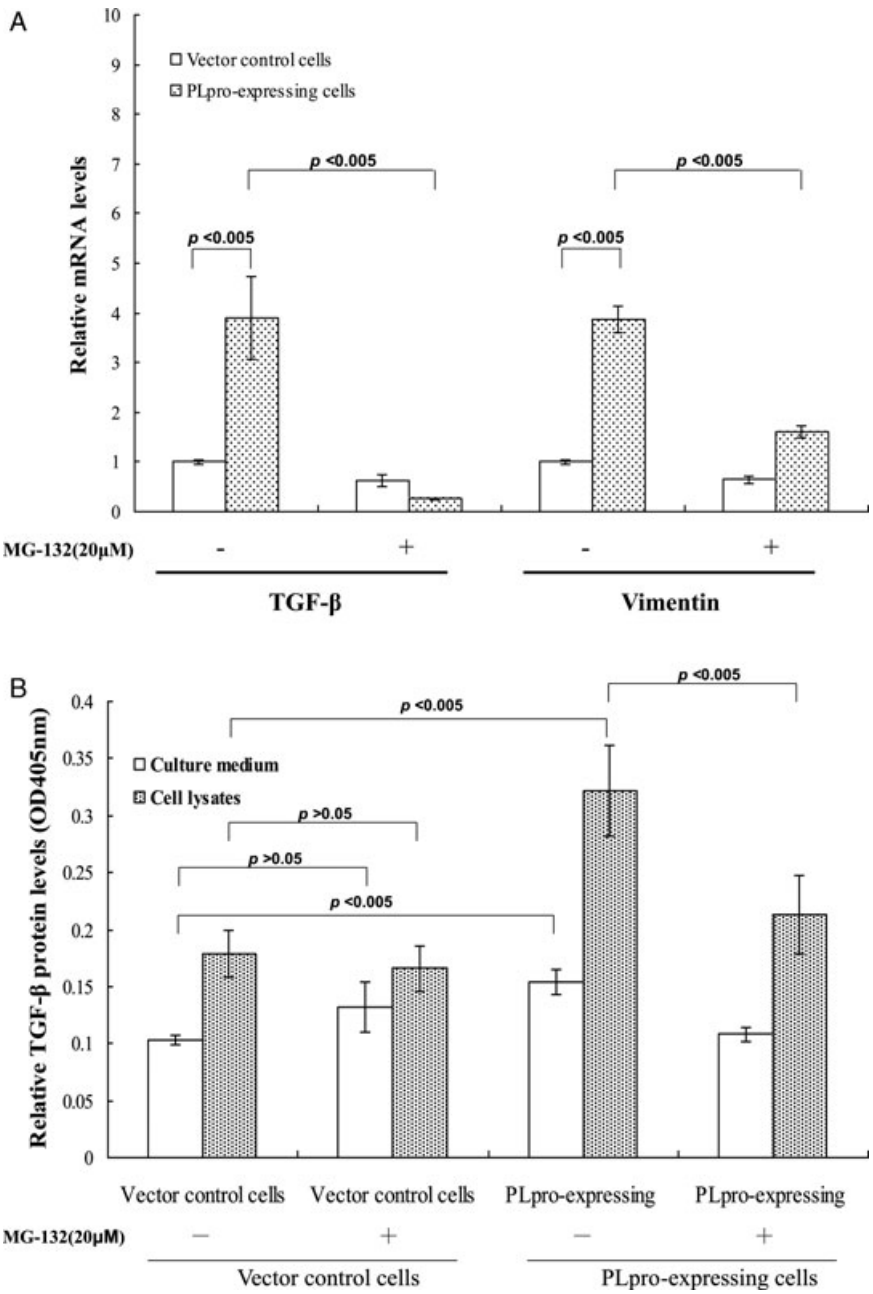

Figure 6. Effect of MG-132 on TGF-β1 and vimentin expression in PLpro-expressing and vector control cells. (A) Vector control or PLpro-expressing cells were treated with or without 20 μM MG-132 for 4 h, mRNA expression of TGF-β and vimentin in untreated or treated cells measured by quantitative PCR and normalized by GAPDH mRNA, presented as relative ratio. (B) Vector control and PLpro-expressing cells treated with or without 20 μM MG-132 were incubated in serum-free media for 1 day. Cultured media or cell lysate were coated into wells of a 96-well plate at 4°C overnight, then reacted with rabbit anti-TGF-β1 antibodies and HRP-conjugated goat antirabbit IgG. The colored product was detected at $OD_{405\ nm}$.

4 Discussion

Rapid elevation of serum cytokines, such as TGF-β1, IL-6, IL-8, IFN-γ, IL-18, IP-10, MCP-1, and MIG, has been detected in SARS patients [6, 7]. Of SARS-CoV proteins, nucleocapsid increased expression of plasminogen activator inhibitor-1 via the Smad3-dependent TGF-β1 signaling pathway [25]. Baculovirus synthesized spike protein activated MAPKs and AP-1, leading to IL-8 release in lung cells [26]. Nonstructure protein 1—but not nonstructured protein 5, envelope, and membrane—induced mRNA expression of CCL5, CXCL10, and CCL3 via activation of NF-κB [27]. This study demonstrated that PLpro-potentiated induction of TGF-β1, IL-1α, and RANTES, particularly inducing more than a threefold increase of TGF-β1 compared to vector controls (Figs. 2A,D, and E and 3). Of these three cytokines, TGF-β1 has been reported to stimulate epithelial–mesenchymal transdifferentiation (EMT) and induced kidney and lung fibrosis [28, 29]. PLpro can trigger the cytokine storm while playing a vital role in SARS-CoV-induced lung damage.

Schematic figure of proteomic profiling induced by SARS-CoV PLpro (Fig. 8) was confirmed by Western blotting, quantitative real-time PCR, and specific inhibitors (Figs 5–7), showing up- and downregulated proteins identified as linked

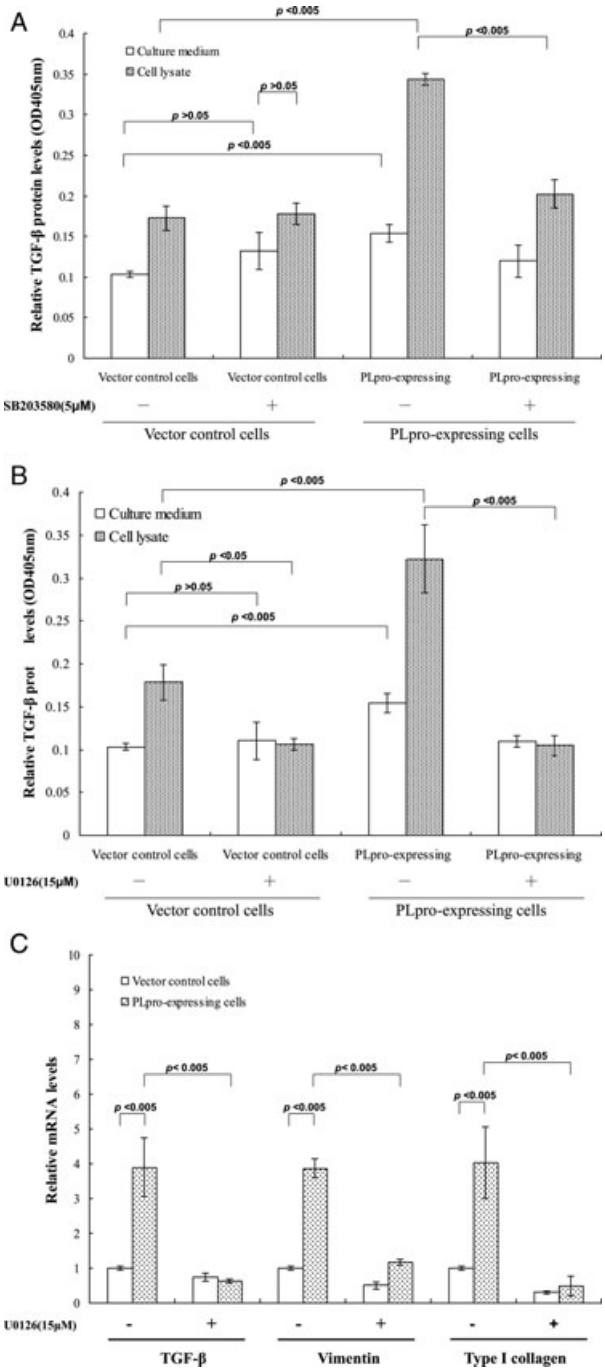

Figure 7. Effect of SB203580 and U0126 on TGF-β1, vimentin, and type I collagen expression in vector control and PLpro-expressing cells. Vector control and PLpro-expressing cells treated with and without (A) 5 μM SB203580 or (B) 15 μM U0126 were incubated in serum-free media for 1 day. Cultured media or cell lysate were coated into wells of a 96-well plate at 4°C overnight, then reacted with rabbit anti-TGF-β1 antibodies and HRP-conjugated goat antirabbit IgG. Colored product was detected at $OD_{405\ nm}$. (C) Vector control or PLpro-expressing cells were treated with and without 15 μM U0126 for 1 day. The mRNA expression of TGF-β1, vimentin, and type I collagen in both types of cells untreated or treated was measured by quantitative PCR, normalized by GAPDH mRNA, presented as relative ratio.

with TGF-β1 production in PLpro-expressing cells. Proteomic analysis indicated PLpro upregulating expression of many TGF-β1-associated genes, e.g. HSP27 (Spot ID 1), vimentin (Spot ID 7), protein disulfide isomerase A3 precursor (Spot ID 11), retinal dehydrogenase 2 (Spot ID 13), glial fibrillary acidic protein (Spot ID 17), glutathione transferase omega-1 (Spot ID 21) (Fig. 8, Table 1). Functional analysis using PANTHER classification system demonstrated PLpro upregulating cytoskeleton proteins such as vimentin (Spot ID 7), T-complex protein 1 subunit epsilon (Spot ID 9), desmoplakin (Spot ID 12), junction plakoglobin (Spot ID 16), glial fibrillary acidic protein (Spot ID 17), and tropomyosin alpha-3 chain (TPM3, Spot ID 18). These cytoskeleton proteins were involved in cell adhesion, cellular component morphogenesis, immune system process, signal transduction, and/or cell motion. Meanwhile, cytoskeleton protein changes and induction of such processes correlated with greater TGF-β1 production by PLpro. Recent reports verified TGF-β1-mediated vimentin upregulation in alveolar epithelial cells as adequate for healing injured lung tissue [23, 24, 30]. Vimentin upregulation was consistent with activation of profibrotic cytokines TGF-β1 induced by SARS-CoV PLpro. Vimentin, HSP27, glial fibrillary acidic protein, retinal dehydrogenase 2, and glutathione transferase omega-1 linked with TGF-β1-induced EMT pathogenesis and fibrosis [23, 24, 31, 32]. Protein disulfide isomerase A3 precursor influenced release and activation of latent TGF-β1 from extracellular matrix [33], whereas glutathione transferase omega-1 polymorphism correlated with expression of TGF-β1 [34].

Biological pathways in Fig. 8 indicate PLpro activating ubiquitin proteasome via upregulation of UBE2K (Spot ID 3) and proteasome subunit alpha type 5 (Spot ID 4), and p38MAPK and ERK1/2 signaling via increase of HSP27 (Spot ID 1). Given proteomic profiling induced by PLpro, we hypothesized the activation of the ubiquitin–proteasomal system, p38 MAPK and ERK1/2 signaled as linked with PLpro-induced upregulation of TGF-β1 and vimentin. Notably, the inhibitor MG-132 treatment confirmed the upregulation of ubiquitin–proteasomal system as involved in PLpro-induced expression of TGF-β1 and vimentin (Fig. 6). Ubiquitin-proteasomal pathway modulated TGF-β1 signaling by regulating expression and activity of effectors in a TGF-β1 signaling cascade [35, 36]. Also, proteasome inhibitor MG-132 would definitely reduce TGF-β1 signaling as well as inhibit activity of Smads and AKT [37, 38], e.g. E3 ubiquitin ligases of ubiquitin–proteasonal system increased ubiquitination and degradation of Smad7 and TGF-β receptor I, which activate p38 MAPK- and JNK-mediated TGF-β1 signaling [39–41]. Inhibiting PLpro-induced expression of TGF-β1 and vimentin by proteasome inhibitor MG-132 support our hypothesis of ubiquitin–proteasonal system as involved in TGF-β1 induction.

The p38 MAPK and ERK1/2 inhibitors (SB203580 and U0126) significantly decreased PLpro-induced expression of TGF-β1, vimentin, and type I collagen (Fig. 7, Table 1), which confirmed p38 MAPK and ERK1/2 modulating PLpro-induced TGF-β1 signaling cascades. Although SARS

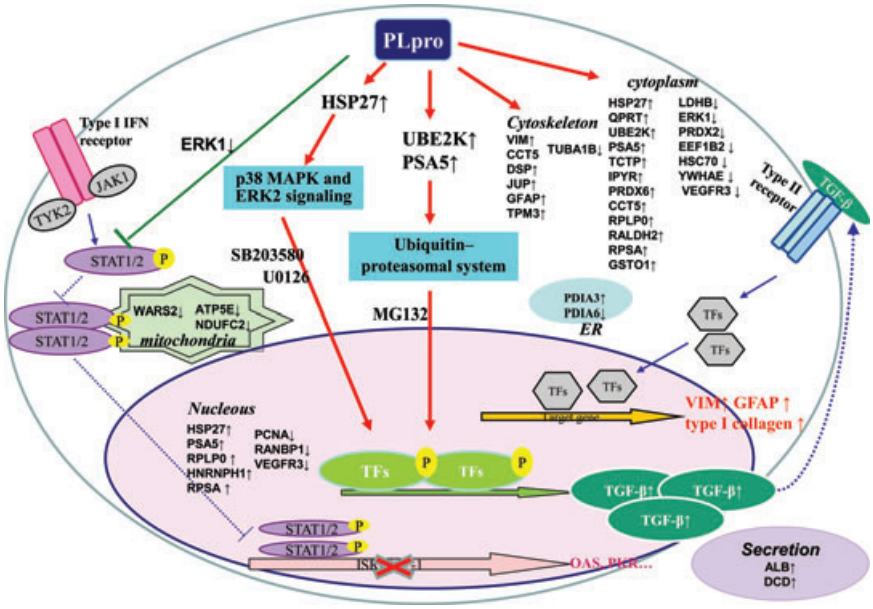

Figure 8. Schematic chart of SARS-CoV PLpro-induced proteomic profile. Up- and downregulated proteins were identified, using 2DE and ESI-Q-TOF, Western blotting, and quantitative PCR, showing activation of p38 MAPK and ERK1/2 signaling pathways, as well as ubiquitin–proteasomal system, as correlated with PLpro-induced TGF-β1 production.

PLpro-enhanced ERK1 degradation via activation of ubiquitin–proteasomal system and inhibited phosphorylation of STAT1 Ser727 in type I IFN signaling pathway, PLpro did not affect amount and activation of ERK2 in human promonocyte cells [16]. ERK2, rather than ERK1, played a key positive role in TGF-β1-mediated EMT marker expression of type I collagen [42, 43]. Other reports proved TGF-β1 inducing EMT and increasing mesenchymal markers (cytokeratins 8 and 19, vimentin, and collagen type α1) via ERK2-dependent signaling in pancreatic cancer cell lines [39]. We suggest ERK2 activation as crucial in PLpro-induced TGF-β1-mediated collagen synthesis, consistent with the previous report [43].

SARS-CoV PLpro, a deubiquitinating enzyme, triggered TGF-β1 production via ubiquitin-proteasomal system, as well as p38 MAPK and ERK1/2 signaling pathways. Proteasome, p38 MAPK, and ERK1/2 inhibitors confirmed correlation between TGF-β1 induction and proteome profiling induced by PLpro. The study highlights a pivotal role of PLpro in both TGF-β1 production and SARS pathogenesis.

We would like to thank the National Science Council (Taiwan) and China Medical University for financial support (NSC101-2320-B-039-036-MY3, CMU98-P-03-M, and CMU99-NSC-08).

The authors have declared no conflict of interest.

5 References

[1] Tsang, K. W., Lam, W. K., Management of severe acute respiratory syndrome: the Hong Kong University experience. *Am J. Resp. Crit. Med.* 2003, *168*, 417–424.

[2] Hsueh, P. R., Chen, P. J., Hsiao, C. H., Yeh, S. H. et al., Patient data, early SARS epidemic, Taiwan. *Emer. Infect. Dis.* 2004, *10*, 489–493.

[3] Nicholls, J. M., Poon, L. L., Lee, K. C., Ng, W. F. et al., Lung pathology of fatal severe acute respiratory syndrome. *Lancet* 2003, *361*, 1773–1778.

[4] Yan, H., Xiao, G., Zhang, J., Hu, Y. et al., SARS coronavirus induces apoptosis in Vero E6 cells. *J. Med. Virol.* 2004, *73*, 323–331.

[5] Wang, W. K., Chen, S. Y., Liu, I. J., Kao, C. L. et al., Temporal relationship of viral load, ribavirin, interleukin (IL)-6, IL-8, and clinical progression in patients with severe acute respiratory syndrome. *Clin. Infect. Dis.* 2004, *39*, 1071–1075.

[6] Huang, K. J., Su, I. J., Theron, M., Wu, Y. C. et al., An interferon-gamma-related cytokine storm in SARS patients. *J. Med. Virol.* 2005, *75*, 185–194.

[7] He, L., Ding, Y., Zhang, Q., Che, X. et al., Expression of elevated levels of pro-inflammatory cytokines in SARS-CoV-infected ACE2+ cells in SARS patients: relation to the acute lung injury and pathogenesis of SARS. *J. Pathol.* 2006, *210*, 288–297.

[8] Rota, P. A., Oberste, M. S., Monroe, S. S., Nix, W. A. et al., Characterization of a novel coronavirus associated with severe acute respiratory syndrome. *Science* 2003, *300*, 1394–1399.

[9] Ziebuhr, J., Molecular biology of severe acute respiratory syndrome coronavirus. *Curr. Opin. Microbiol.* 2004, *7*, 412–419.

[10] Barretto, N., Jukneliene, D., Ratia, K., Chen, Z. et al., The papain-like protease of severe acute respiratory syndrome coronavirus has deubiquitinating activity. *J. Virol.* 2005, *79*, 15189–15198.

[11] Lindner, H. A., Fotouhi-Ardakani, N., Lytvyn, V., Lachance, P. et al., The papain-like protease from the severe acute

respiratory syndrome coronavirus is a deubiquitinating enzyme. *J. Virol.* 2005, *79*, 15199–15208.

[12] Sulea, T., Lindner, H. A., Purisima, E. O., Menard, R., Deubiquitination, a new function of the severe acute respiratory syndrome coronavirus papain-like protease? *J. Virol.* 2005, *79*, 4550–4551.

[13] Ratia, K., Saikatendu, K. S., Santarsiero, B. D., Barretto, N. et al., Severe acute respiratory syndrome coronavirus papain-like protease: structure of a viral deubiquitinating enzyme. *Proc. Natl. Acad. Sci. USA* 2006, *103*, 5717–5722.

[14] Spiegel, M., Pichlmair, A., Martinez-Sobrido, L., Cros, J. et al., Inhibition of beta interferon induction by severe acute respiratory syndrome coronavirus suggests a two-step model for activation of interferon regulatory factor 3. *J. Virol.* 2005, *79*, 2079–2086.

[15] Frieman, M., Ratia, K., Johnston, R. E., Mesecar, A. D., Baric, R. S., Severe acute respiratory syndrome coronavirus papain-like protease ubiquitin-like domain and catalytic domain regulate antagonism of IRF3 and NF-kappaB signaling. *J. Virol.* 2009, *83*, 6689–6705.

[16] Li, S. W., Lai, C. C., Ping, J. F., Tsai, F. J. et al., Severe acute respiratory syndrome coronavirus papain-like protease suppressed alpha interferon-induced responses through downregulation of extracellular signal-regulated kinase 1-mediated signalling pathways. *J. Gen. Virol.* 2011, *92*, 1127–1140.

[17] Kovalenko, A., Chable-Bessia, C., Cantarella, G., Israel, A. et al., The tumour suppressor CYLD negatively regulates NF-kappaB signalling by deubiquitination. *Nature* 2003, *424*, 801–805.

[18] Liu, S., Lv, J., Han, L., Ichikawa, T. et al., A pro-inflammatory role of deubiquitinating enzyme cylindromatosis (CYLD) in vascular smooth muscle cells. *Biochem. Biophys. Res. Commun.* 2012, *420*, 78–83.

[19] Parvatiyar, K., Harhaj, E. W., Regulation of inflammatory and antiviral signaling by A20. *Microbes Infect.* 2011, *13*, 209–215.

[20] Lai, C. C., Jou, M. J., Huang, S. Y., Li, S. W. et al., Proteomic analysis of up-regulated proteins in human promonocyte cells expressing severe acute respiratory syndrome coronavirus 3C-like protease. *Proteomics* 2007, *7*, 1446–1460.

[21] Yu-Jen Jou, Y-J., Lin, C-D., Lai, C-H., Chen, C-H. et al., Proteomic identification of salivary transferrin as a biomarker for early detection of oral cancer. *Anal. Chim. Acta* 2010, *681*, 41–48.

[22] Yang, T. C., Lai, C. C., Shiu, S. L., Chuang, P. H. et al. Japanese encephalitis virus down-regulates thioredoxin and induces ROS-mediated ASK1-ERK/p38 MAPK activation in human promonocyte cells. *Microbes Infect.* 2010, *12*, 643–651.

[23] Mi, H., Dong, Q., Muruganujan, A., Gaudet, P. et al. PANTHER classification system version 7: improved phylogenetic trees, orthologs and collaboration with the Gene Ontology Consortium. *Nucleic Acids Res.* 2010, *38*, D204–D210.

[24] Thomas, P. D., Kejariwal, A., Campbell, M. J., Mi, H. et al. PANTHER: a browsable database of gene products organized by biological function, using curated protein family and subfamily classification. *Nucleic Acids Res.* 2003, *31*, 334–341.

[25] Zhao, X., Nicholls, J. M., Chen, Y. G., Severe acute respiratory syndrome-associated coronavirus nucleocapsid protein interacts with Smad3 and modulates transforming growth factor-beta signaling. *J. Biol. Chem.* 2008, *283*, 3272–3280.

[26] Chang, Y. J., Liu, C. Y., Chiang, B. L., Chao, Y. C., Chen, C. C., Induction of IL-8 release in lung cells via activator protein-1 by recombinant baculovirus displaying severe acute respiratory syndrome-coronavirus spike proteins: identification of two functional regions. *J. Immunol.* 2004, *173*, 7602–7614.

[27] Law, A. H., Lee, D. C., Cheung, B. K., Yim, H. C., Lau, A. S., Role for nonstructural protein 1 of severe acute respiratory syndrome coronavirus in chemokine dysregulation. *J. Virol.* 2007, *81*, 416–422.

[28] Willis, B. C., Borok, Z., TGF-beta-induced EMT: mechanisms and implications for fibrotic lung disease. *Am. J. Physiol. Lung Cell. Mol. Physiol.* 2007, *293*, L525–L534.

[29] Iwano, M., EMT and TGF-beta in renal fibrosis. *Front Biosci. (Schol. Ed.)* 2010, *2*, 229–238.

[30] Rogel, M. R., Soni, P. N., Troken, J. R., Sitikov, A. et al., Vimentin is sufficient and required for wound repair and remodeling in alveolar epithelial cells. *FASEB J.* 2011, *25*, 3873–3883.

[31] Georgiadis, A., Tschernutter, M., Bainbridge, J. W., Balaggan, K. S. et al., The tight junction associated signalling proteins ZO-1 and ZONAB regulate retinal pigment epithelium homeostasis in mice. *PLoS One* 2010, *5*, e15730.

[32] Xu, C., Chen, Z. X., Liu, W. Y., Wang, Y. X., Xiong, Z. X., A series of observation on the expression of TGF-beta1 in the lung of nitrofen-induced congenital diaphragmatic hernia rat model. *Zhonghua Wai Ke Za Zhi* 2009, *47*, 301–304.

[33] Boyan, B. D., Schwartz, Z., 1,25-Dihydroxy vitamin D3 is an autocrine regulator of extracellular matrix turnover and growth factor release via ERp60-activated matrix vesicle matrix metalloproteinases. *Cells, Tissues, Organs* 2009, *189*, 70–74.

[34] Escobar-Garcia, D. M., Del Razo, L. M., Sanchez-Pena, L. C., Mandeville, P. B. et al., Association of glutathione S-transferase Omega 1–1 polymorphisms (A140D and E208K) with the expression of interleukin-8 (IL-8), transforming growth factor beta (TGF-beta), and apoptotic protease-activating factor 1 (Apaf-1) in humans chronically exposed to arsenic in drinking water. *Arc. Toxicol.* 2012, *86*, 857–868.

[35] Weiss, C. H., Budinger, G. R., Mutlu, G. M., Jain, M., Proteasomal regulation of pulmonary fibrosis. *Proc. Am. Thorc. Soc.* 2010, *7*, 77–83.

[36] Pan, X., Hussain, F. N., Iqbal, J., Feuerman, M. H., Hussain, M. M., Inhibiting proteasomal degradation of microsomal triglyceride transfer protein prevents CCl4-induced steatosis. *J. Biol. Chem.* 2007, *282*, 17078–17089.

[37] Hofer, E. L., La Russa, V., Honegger, A. E., Bullorsky, E. O. et al., Alteration on the expression of IL-1, PDGF, TGF-beta, EGF, and FGF receptors and c-Fos and c-Myc proteins in bone marrow mesenchymal stroma cells from advanced untreated lung and breast cancer patients. *Stem Cells Dev.* 2005, *14*, 587–594.

[38] Fukasawa, H., Yamamoto, T., Togawa, A., Ohashi, N. et al., Down-regulation of Smad7 expression by ubiquitin-dependent degradation contributes to renal fibrosis in obstructive nephropathy in mice. *Proc. Natl. Acad. Sci. USA* 2004, *101*, 8687–8692.

[39] Hayashi, H., Abdollah, S., Qiu, Y., Cai, J. et al., The MAD-related protein Smad7 associates with the TGF-beta receptor and functions as an antagonist of TGF-beta signaling. *Cell* 1997, *89*, 1165–1173.

[40] Soond, S. M., Chantry, A., How ubiquitination regulates the TGF-beta signalling pathway: new insights and new players: new isoforms of ubiquitin-activating enzymes in the E1-E3 families join the game. *Bioessays* 2011, *33*, 749–758.

[41] Ellenrieder, V., Hendler, S. F., Boeck, W., Seufferlein, T. et al., Transforming growth factor beta1 treatment leads to an epithelial-mesenchymal transdifferentiation of pancreatic cancer cells requiring extracellular signal-regulated kinase 2 activation. *Cancer Res.* 2001, *61*, 4222–4228.

[42] Li, F., Ruan, H., Fan, C., Zeng, B. et al., Efficient inhibition of the formation of joint adhesions by ERK2 small interfering RNAs. *Biochem. Biophys. Res. Commun.* 2010, *391*, 795–799.

[43] Li, F., Zeng, B., Chai, Y., Cai, P. et al., The linker region of Smad2 mediates TGF-beta-dependent ERK2-induced collagen synthesis. *Bioche. Biophys. Res. Commun.* 2009, *386*, 289–293.

